minerals

MDPI

Article

Iron-Speciation Control of Chalcopyrite Dissolution from a Carbonatite Derived Concentrate with Acidic Ferric Sulphate Media

Kolela J. Nyembwe [1,2], Elvis Fosso-Kankeu [1,3,*], Frans Waanders [1] and Martin Mkandawire [1,2,*]

1 Water Pollution Monitoring and Remediation Initiative Research Group in the Centre of Excellence of Carbon-Based Fuels, North-West University, Potchefstroom 2520, South Africa; djosnyembwe@gmail.com (K.J.N.); frans.waanders@nwu.ac.za (F.W.)
2 Department of Chemistry, School of Science and Technology, Cape Breton University, Sydney, NS B1P 6L2, Canada
3 Department of Electrical and Mining Engineering, College of Science Engineering and Technology, Florida Science Campus, University of South Africa, Florida Park, Roodepoort 1709, South Africa
* Correspondence: fossoe@unisa.ac.za (E.F.-K.); martin_mkandawire@cbu.ca (M.M.); Tel.: +1-902-563-1430 (M.M.)

Abstract: The mechanisms involved in the dissolution of chalcopyrite from a carbonatite concentrate in a ferric sulphate solution at pH 1.0, 1.5 and 1.8, and temperatures 25 °C and 50 °C were investigated. Contrary to expectations and thermodynamic predictions according to which low pH would favour high Cu dissolution, the opposite was observed. The dissolution was also highly correlated to the temperature. $CuFeS_2$ phase dissolution produced intermediate Cu rich phases: CuS, Cu_2S and Cu_5FeS_4, which appeared to envelop $CuFeS_2$. Thermodynamic prediction revealed CuS to be refractory and could hinder dissolution. $CuFeS_2$ phase solid-state dissolution process was further discussed. Free $Fe_3{}^+$ and its complexes $(Fe(HSO_4)_2{}^+$, $Fe(SO_4)^{2-}$ and $FeSO_4{}^+$ were responsible for Cu dissolution, which increased with increasing pH and temperature. The dissolution improved at pH 1.8 rather than 1.0 due to the increase of $(Fe(HSO_4)^{2+}$, $Fe(SO_4)^{2-}$ and $FeSO_4{}^+$, which were also the predominating species at a higher temperature. The fast and linear first dissolution stage was attributed to the combined effect of Fe^{3+} and its complex $(Fe(HSO_4)^{2+}$, while $Fe(SO_4)^{2-}$ was the main species for the second Cu dissolution stage characterised by a slow rate.

Keywords: hydrometallurgy; carbonatitic chalcopyrite; copper; speciation phases; intermediate phases

Citation: Nyembwe, K.J.; Fosso-Kankeu, E.; Waanders, F.; Mkandawire, M. Iron-Speciation Control of Chalcopyrite Dissolution from a Carbonatite Derived Concentrate with Acidic Ferric Sulphate Media. *Minerals* **2021**, *11*, 963. https://doi.org/10.3390/min11090963

Academic Editor: Kenneth N. Han

Received: 26 July 2021
Accepted: 26 August 2021
Published: 3 September 2021

1. Introduction

The demand for copper (Cu) has risen over the past few decades due to the rapid growth of the electronic industry. A major source of Cu is chalcopyrite ($CuFeS_2$), a copper sulphide mineral, which accounts for around 70–80% of the total global production of Cu. The pyrometallurgy route produces about 85% of worldwide Cu through a reverberatory furnace or flash smelting [1]. However, this process is becoming expensive due to ever-increasing stringent environmental regulations coupled with abnormal SO_2 emissions and the huge volume of tailings generated through froth flotation. For instance, for every ton of copper obtained through flotation processes, 151 tonnes of tailings are produced [2]. On the other hand, the relative decrease in profit margins for mineral processing caused by the scarcity of high-grade ore bodies is also a concern. Consequently, hydrometallurgy can be economically attractive for the production of Cu from $CuFeS_2$ and present several advantages, including high selectivity, environmental friendliness, suitable for low or complex chalcopyrite ore bodies [3].

Hydrometallurgy is the extraction of minerals from the ore by leaching with aqueous solvents (*aka* medium). Some of the solvents for $CuFeS_2$ include sulphate-based media (H_2SO_4-$Fe_2(SO_4)_3$) [4], chloride-based media (HCl-$FeCl_3$) [5], mixed chloride-sulphate

media (H_2SO_4-$Fe_2(SO_4)_3$-NaCl) [6] and nitrate-based media ($Fe(NO_3)_3$) [7]. CuFeS2 is highly refractory and regarded as one of the most difficult minerals to leach regardless of the media. Its leaching is slow and incomplete due to the formation of a diffusion barrier that builds up between the leaching solution and $CuFeS_2$. The nature and composition of this barrier, together with the dissolution mechanism, still remain controversial [4,8,9]. There are three hypotheses regarding the structure of the formed diffusion barrier. The first hypothesis is that elemental sulphur (S^0), formed during leaching, prevents further diffusion of the reactant from reaching the un-leached chalcopyrite [10,11]. The second hypothesis, commonly cited, attributes it to the formation of Cu-rich polysulphides, formed due to solid-state transformation through the preferential Fe dissolution. This hypothesis is referred to as the metal-deficient sulphide theory [12,13]. The third hypothesis refers to iron-precipitates jarosite, jarosite-like species and goethite [13,14].

According to the Eh-pH (Pourbaix) diagram (Figure S1) for the Cu-Fe-S-H_2O system, dissolution of $CuFeS_2$ in acidic media takes place through a solid transformation in different intermediate sulphide (Cu_5FeS_4, CuS and Cu_2S) phases. The formation of these phases may, to some extent, be attributed to the slow chemical kinetics associated with the products of the reaction. The diagram also shows that successful copper dissolution from the mineral could be achieved after increasing the redox potential above 0.44 V (SHE) [10]. Consequently, acidic ferric sulphates (H_2SO_4-$Fe_2(SO_4)_3$-$FeSO_4$-H_2O) are gaining prominence as preferred dissolution media for the chalcopyrite leaching process in hydrometallurgical extraction of Cu. The H_2SO_4-$Fe_2(SO_4)_3$-$FeSO_4$-H_2O presents several advantages, including its simple chemistry, low capital and operational costs and environmental friendliness [15]. In this media, Fe is distributed as free Fe^{3+} and Fe^{2+} and or as complexed iron compounds (e.g., $FeHSO_4^+$, $FeSO_4^0$, $Fe(HSO_4)^{2+}$, $Fe(SO_4)^{2-}$ and $FeSO_4^+$) and their content in solution depend on the pH and temperature [16,17]. The thermodynamic function and equilibrium constant of the various species are presented in Table S1 (supplementary information). Therefore, the oxidising power/strength of H_2SO_4-$Fe_2(SO_4)_3$-$FeSO_4$-H_2O solution must be viewed as a function of all the possible ferric species present in the solution. Hirato and co-workers [18] examined the speciation of (H_2SO_4-$Fe_2(SO_4)_3$-$FeSO_4$-H_2O) and plotted the distribution of Fe species according to Sapieszko et al. [19] and concluded that Fe^{3+} and $FeHSO_4^{2+}$ are the important Fe species for the $CuFeS_2$ dissolution in H_2SO_4-$Fe_2(SO_4)_3$-$FeSO_4$-H_2O.

The leaching kinetics may be related to the distribution of iron species in the solution. In addition, the inherent problem with the direct application of Eh-pH diagrams (Figure S1) to leaching is the possible formation of intermediate phases, and there is no way to predict the presence of metastable phases from thermodynamics considerations alone. Nevertheless, a comprehensive $CuFeS_2$ dissolution mechanism could be obtained by systematic leached residue characterization employing surface analytical methods (such as X-ray photoelectron spectroscopy, X-ray absorption spectroscopy, X-ray diffraction, scanning electron microscope and Raman spectroscopy) and through control of solution chemical aspects, among which the solution redox and pH are very important.

Most previous studies reporting on the Cu recoveries from $CuFeS_2$ only characterized solids residue at the resolved experimental end time. This has not allowed for evaluating the entire mineral phase evolution taking place during dissolution. This work, therefore, conducts the dissolution of $CuFeS_2$ in H_2SO_4-$Fe_2(SO_4)_3$-$FeSO_4$-H_2O system at different pH regimes (1.0, 1.5 and 1.8) and operating temperatures (25 °C and 50 °C) and identify the likely refractory intermediates based on the solid-state transformation taking place throughout the dissolution process. Furthermore, it investigates the evolution of Fe species during $CuFeS_2$ leaching in H_2SO_4-$Fe_2(SO_4)_3$-$FeSO_4$-H_2O.

2. Materials and Methods

2.1. Materials

Solutions of the desired pH were prepared using analytical grade sulphuric acid (H_2SO_4 98% A.C.E.), ferric sulphate ($Fe_2(SO_4)_3 \cdot H_2O$ A.C.E.), and deionised water

(<5.0 µs/cm). The measured redox potential (Ag/AgCl) measurements were referenced to the Standard Hydrogen Electrode (SHE).

2.2. Chalcopyrite Sample Preparation and Characterisation

The chalcopyrite concentrate samples were obtained from a carbonatitic ore body treated through flotation at Phalaborwa Copper Mining Company (Limpopo Province, South Africa). Its major phases were chalcopyrite ($CuFeS_2$ (68.37%)), Mg-rich calcite (Mg-$CaCO_3$ (29.27%)) and traces of another copper sulphide (Cu_7S_4 (3.41%), Cu_9S_5 (2.51%) and Cu_5FeS_4(4.51)) with quartz (SiO_2 (2.20)) (Figure S2). The sample had a bulk Cu content of 36.39% and was dried in an oven at 50 °C for seven days before sub-sampling. First, the homogenisation of samples was carried out according to the soil sampling protocol by the U.S. Environmental Protection Agency [20]. Then, approximately 0.5 kg of concentrate was sub-sampled and further dried for 2 h at 105 °C. The grains with sizes smaller than 200 µm were used as the dissolution feed at an average grain size of 32 µm (Figure S2d). The powdered sample was characterised in an earlier study by Nyembwe et al. [21] for its chemistry, mineral composition and morphology using the XRF, X-ray diffraction (XRD) and scanning electron microscopy–energy dispersive spectroscopy (SEM-EDX), respectively. They are provided in Supplementary Information Figure S2.

2.3. Leaching Media and Tests

The $CuFeS_2$ dissolution was conducted in acidified ferric sulphate solution (H_2SO_4-$Fe_2(SO_4)_3$), obtained by mixing $Fe_2(SO_4)_3$ with H_2O water and H_2SO_4. An initial Fe content (Fe^{3+} = 0.05 M Fe) was used for all tests. The media was agitated for 12 h prior to use. Dissolution tests were performed at atmospheric conditions at 25 °C or 50 °C. The media pH was measured and maintained at 1.0, 1.5 and 1.8 with periodic addition of H_2SO_4 (98%) while the solution's oxidation reduction potential (ORP) could evolve throughout the dissolution test. An initial pulp density of 10% was used in all tests, with 40 g of the dried chalcopyrite sample mixed with 400 mL of the leaching liquor in a 600 mL Erlenmeyer flask (conical wide neck). The agitation (500 rpm) was achieved through use of an overhead stirred (stirrer ES, Velp Scientica (0–1300 pm)) placed on top of the dissolution vessel (Figure S3). An initial pulp density of 10% was used in all tests, with 40 g of the dried chalcopyrite sample mixed with 400 mL of the leaching liquor in a 600 mL Erlenmeyer flask. 10 mL sample was withdrawn every 20 min for chemical analysis, while the solution ORP was measured at intervals and converted to the SHE. Total Cu and Fe were analysed using atomic absorption flame spectrometry (AAFS, Thermo Scientific ICE 3000 series).

2.4. Leachate Speciation

Chemical Fe speciation was calculated using the geochemical modelling software, PhreeqC (version 3.3.12-12704, U.S. Geological Survey). Fe speciation and its evolution throughout the dissolution were based on the initial (prepared medium) characterization and each withdrawn leachate solution. The characterization of each solution involved the determination of total cations, sulphates (SO_4^{2-}), pH, Eh (Ag/AgCl), T (°C), and solution density (ρ). These measurements were used as individual inputs (data block of interest), inserted for Fe leachate speciation modelling. Each solution was considered an independent data block (master species with inputs of the measured concentration, pH, Eh and temperature) from which the curves of the aqueous Fe species were obtained and drawn.

The software is based on an ion association aqueous model. The equilibrium speciation is defined by a set of equations governed by element mass balance electrical charge balance [18]. The redox chemistry is defined by Equation (1), which is based on the electron activity whereby R is the gas constant (8.314 JK^{-1} mol^{-1}), T is the temperature (K), F represents the Faraday constant (96,485 C mol^{-1}), pE negative log of the electron activity (equilibrium position for all redox couples in the system), which is related to Eh and delivered using Equation (1).

$$Eh = pE(2.302 \times R \times T)/F \quad (1)$$

2.5. Residue Characterisation

Solid were analysed for mineral composition using XRD and optical phase identification and surface morphology using SEM–EDX. The XRD analysis using a Rigaku Ultima IV (Rigaku Corporation, Tokyo, Japan) was operated at 40 kV and 30 mA. PDXL analysis software was used, and the instrument's detection limit was 2%. Data were recorded over the range $5° \leq 2\theta \leq 95°$ at a scan rate of 0.5°/min and step width of 0.01°. Tescan S.E.M. (operated at 20 kV) with E.D.X. analysis was used for grain morphology and chemistry. Residues were carbon-coated prior to analysis.

3. Results and Discussion

3.1. Initial Fe Speciation of the Media

The initial Fe speciation at pH 1.0, 1.5 and 1.8 at 25 or 50 °C was simulated using PhreeqC and is shown in Figure 1. Fe^{2+} and $Fe(HSO_4)^+$ were the main iron species observed (Figure 1a) at all the pH and temperatures. The increase in pH and temperature appears to have slightly increased the concentration of Fe^{3+} and its sulphate complexes ($Fe(HSO_4)^{2+}$, $Fe(SO_4)^{2-}$ and $FeSO_4^+$) to the expense of free Fe^{2+} (Figure 1a) even much more with the increase of temperature 25–50 °C (Figure 1b). The high ORP and *pE* support this at higher pH or temperature. *pE* values at 25 °C were 9.3, 9.41 and 9.57 at a pH of 1.0, 1.5 and 1.8, respectively. While at 50 °C, *pE* values of 9.51, 9.7 and 9.86 were recorded.

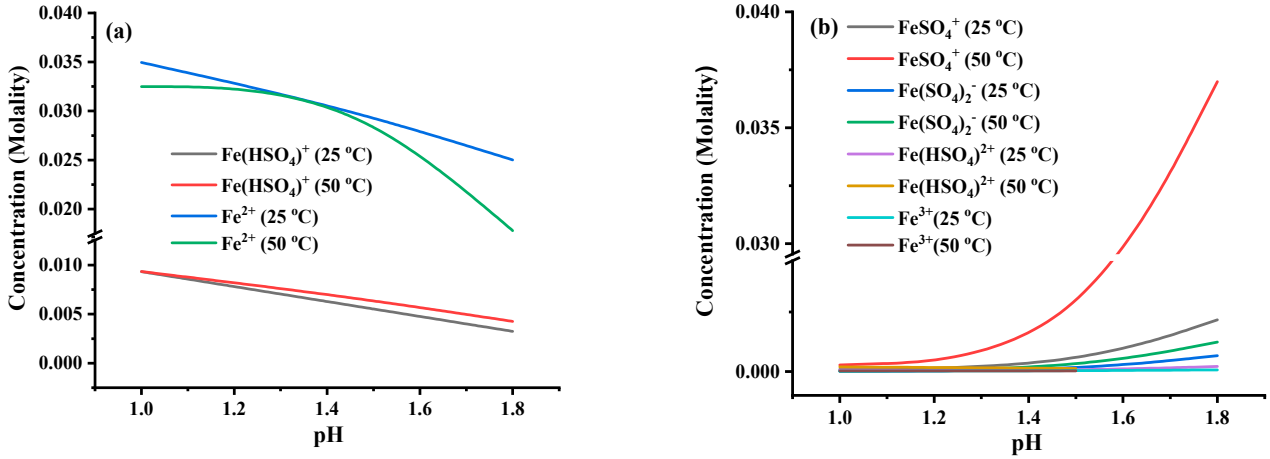

Figure 1. Initial Fe speciation at the various pH regimes (1.0, 1.5 and 1.8) and temperatures vis 25 and 50 °C, where (**a**) shows speciation of Fe^{2+} and (**b**) is the speciation of Fe^{3+}.

3.1.1. Cu Dissolution Rate and Recovery

The leaching of $CuFeS_2$ at different temperatures under variable pH of media is presented in Figure 2. More Cu dissolved at 50 °C than at 25 °C and slightly more at pH 1.8 than 1.5 and 1.0 (evident at 50 °C, not so at 25 °C). It can be seen that pH plays an essential role in the dissolution of $CuFeS_2$. Previous reports suggest that an acidic environment minimises hydrolysis and ferric precipitation. The obtained recoveries agreed with Antonijevic and Bogdanovic [22], and Córdoba et al. [23] point out that chalcopyrite easily oxidises at higher pH values when oxygen is present in solutions.

All dissolution curves were asymptotic and characterised by three stages: the first was more rapid (from 0–60 min) than the second (40–360 min), and the third was a plateau with no Cu dissolution (360–720 min). Our results support those of Klauber et al. [10] and Salinas et al. [24], but not those of Jones and Peters [25], who observed a linear kinetic probably due to an extended dissolution time over 55 days. The form of the dissolution curve showed the plateau is reached around 380–420 min of dissolution at room temperature (i.e., 25 °C). While at 50 °C, the maximum Cu recovery is reached after 180–220 min of dissolution,

which could be attributed to a more rapid reaction at higher temperatures and formation of the reaction products.

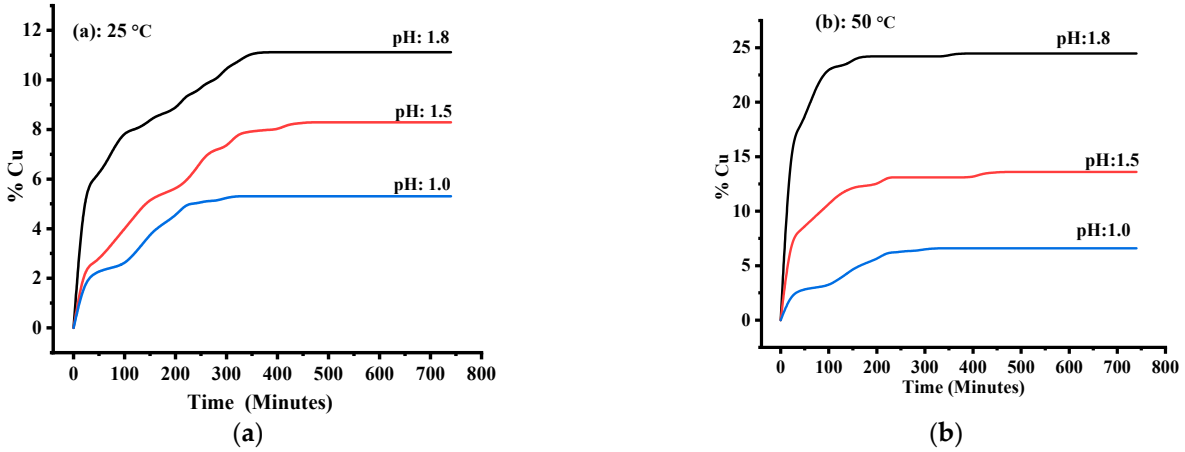

Figure 2. Isotherms of chalcopyrite dissolution and recovery of Cu in leachates using media with different pH values and conducted at (**a**) 25 °C and (**b**) 50 °C.

3.1.2. Ferric Speciation during Chalcopyrite Leaching

The leaching of Cu from the chalcopyrite mineral over a time spate is presented in Figure 3, which also shows the evolution of Fe speciation at 50 °C for different pH. Speciation was calculated using the measured total Fe and Cu in the solution and the recorded redox potential. It was observed that the initial concentration of Fe^{3+} and its complexes dropped during Cu dissolution, which suggests that Fe^{3+} is not the only species responsible for $CuFeS_2$ oxidation.

Fe^{3+} and $Fe(HSO_4)^{2+}$ both linearly dropped within the first 40 or 80 min (Figure 3a,b) of the Cu dissolution while the Cu recovery curve continued over 200 min (Figure 3a,b). At 25 °C, Fe^{3+} decreased by 90, 67 and 78% at pH 1.0, 1.5 and 1.8. While at 50 °C, its content decreased further by 97, 82 and 87, respectively. $Fe(HSO_4)^{2+}$ also decreased by 17, 28 57% at 25 °C. At 50 °C, its content went down by 32, 51 and 71%. Our results support Hirato et al. [26], who concluded that Fe^{3+} and $Fe(HSO_4)^{2+}$ play a significant role during ferric leaching of $CuFeS_2$. Our results show that the initial fast rapid and linear Cu dissolution stage corresponds to the combined effect of Fe^{3+} and $Fe(HSO_4)^{2+}$.

The increase in pH from 1.0~1.8 led to an increase in $Fe(SO_4)^{2-}$ content (Figure 2b). At pH 1.8, for instance, this species appeared to be the dominant form of Fe(III) in solution after the $FeSO_4^+$. The results showed that $Fe(SO_4)^{2-}$ decreased during Cu leaching from its initial content by 15 and 85%, respectively, at 25 and 50 °C. Its decrease was gradual and prolonged over 300 min (Figure 3c) and could correspond to the second dissolution stage (from 80 to 340 min), characterised by a relatively low rate than the first stage. Thus, implying that $Fe(SO_4)^{2-}$ contributed to Cu dissolution. $FeSO_4^+$ also decreased to a less extent within the first 40 min of leaching. Its content went down at 25 °C by 7, 16 and 24, further by 28, 35 and 41% at 50 °C. The speciation results further revealed that the decrease rate of the various Fe(III) species and Fe(II) increase matches the Cu dissolution rate.

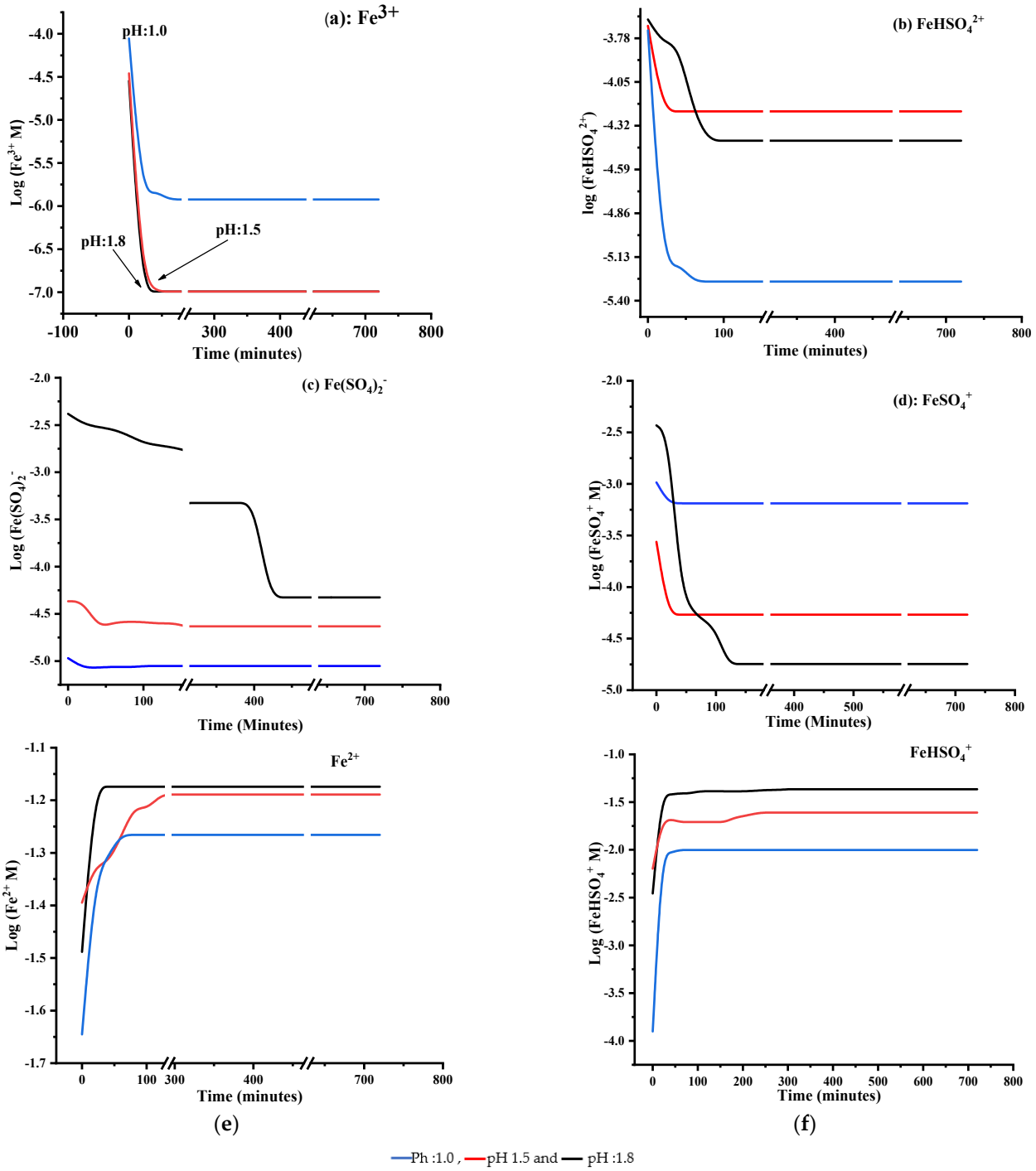

Figure 3. Fe speciation at different pH (1.0, 1.5 and 1.8) at 250 °C. (**a**) displaying the evolution of Fe^{3+}, (**b**) $Fe(HSO_4)^{2+}$, (**c**) $Fe(SO_4)^{2-}$, (**d**) $FeSO_4^+$, (**e**) Fe^{2+}, and (**f**) $FeHSO_4^+$.

3.1.3. Effect of Temperature

Raising the temperature revealed a positive response to the rate of metal dissolution and recovery during the dissolution process. Its effect appeared to be pronounced when the temperature was increased from 25 to 50 °C (Figure 3b). Previous studies have reported that more than ten times the extraction of Cu has been identified when dissolving $CuFeS_2$ by raising the temperature from 30 to 90 °C [12]. The obtained results support the improved Cu leaching. For instance, at 50 °C and pH 1.8, the Cu dissolution rate doubled, while at

1.5 and 1.0, it increased by a factor of 1.6 and 1.2, respectively. Thus, it supports the positive impact of temperature upon mineral dissolution.

3.2. Effect of Initial Solution Potential

It should be worth noting that the initial solution oxido-reduction potential (ORP) varied according to the solution pH, probably due to the various Fe species distribution existing at the different pH values (Figure 1), which also play a major role in the Cu recovery different pH values. At both temperatures, it was observed that high pH (1.8) media possessed a high initial ORP value. In all cases, the initial ORP values showed a similar trend, which decreased at the early dissolution stage and then remained steady till the end of the leaching. At 25 °C, A decline from 550.25 to 52931 mV, 556.183 to 547.362 mV, and 566.434 to 539.1600 mV was recorded for the solution-free pH 0.5, 1.0, 1.5 and 1.8 respectively. While at 50 °C, their initial ORP value decreased from 608 to 572 mV, 621 to 588 mV, and 631 to 591 mV individually. This decrease could suggest the direct oxidation of that mineral by ferric species, increasing the solution's ferrous content. Earlier studies showed the existence of a potential range interval, referred to as critical (400–450 mV Ag/AgCl corresponding to 600–660 CEH approximately while using the conversion as published by Stringgow), [27] in which optimum copper recoveries are obtained [28,29]. Except for the dissolution at pH 1.8, which was within the range and quickly dropped (after 40 min of leaching), all the pH conditions ORP values (pH: 1.0 and 1.5) were well below the critical potential range and could support the low recoveries observed under the various pH regimes and could support the importance of maintaining the solution potential within the stipulated range for the efficient dissolution process.

3.3. Effect of Initial Fe^{3+}

Figure 4 shows copper extraction as a function of time for initial concentrations of Fe^{3+} ions up to 0.075 M at pH 1.8 and temperature 25 °C or 50 °C. The results show that an improved rate and recovery are observed with an increase in Fe^{3+}. The results(Table 1) revealed key kinetic information and showed that Cu recovery depends on Fe^{3+} at first order and with a rate law of $r = [Fe^{3+}]^{0.979}$ within 0.025 to 0.075 M ferric sulphate. These results support Veloso et al. [6], who observed an increase in Cu extraction with increasing Fe^{3+} up to 0.5 M and observed no further increase at 1.0 M Fe^{3+}. Unlike Córdoba et al. [20], who highlighted from past studies that $CuFeS_2$ dissolution rate is strongly affected by Fe^{3+} only at low concentrations. In contrast, at high concentration, its effect is negligible, and no clear kinetic effect with ferric content higher than 0.01 M. The findings of the present work show the first-order dependency up to 0.075 M.

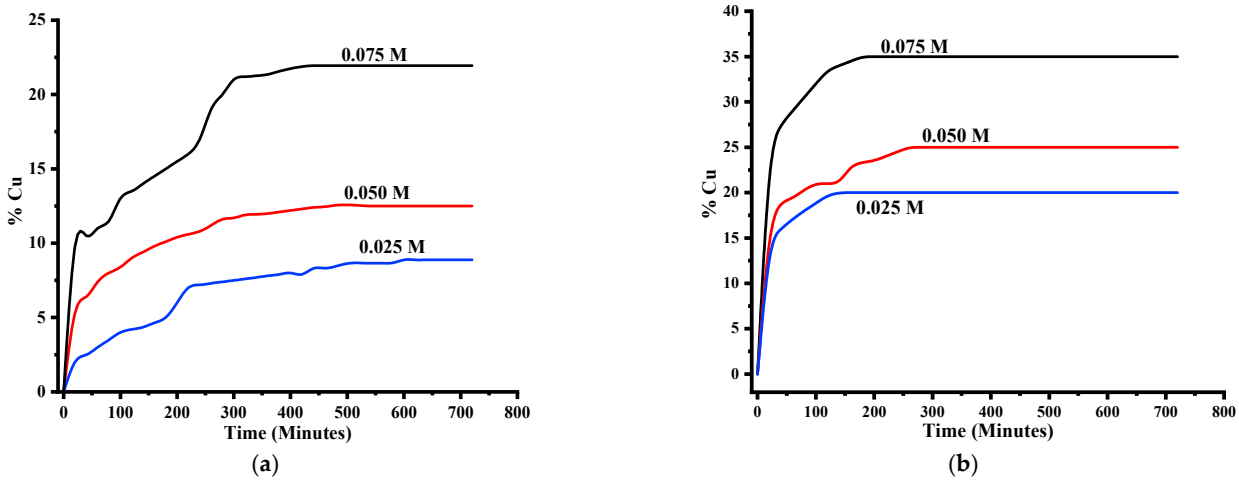

Figure 4. Effect of Fe^{3+} on Cu dissolution (rate and recovery): (**a**) dissolution at 25 °C and (**b**) dissolution at 50 °C.

Table 1. Kinetic parameters of $CuFeS_2$ leaching in Fe^{3+}.

T (K)	$Fe_2(SO_4)_3$ (M)	Rate Cu^{2+}	K $M^{-1}S^{-1}$	Rxt^0 Order Fe^{3+}	Ea (kJ/mol)
298.15	0.025	8.31×10^{-5}	3.3×10^{-3}	0.979	79.04
	0.050	1.61×10^{-4}	3.2×10^{-3}		
	0.075	2.45×10^{-4}	3.3×10^{-3}		
323.5	0.025	9.70×10^{-4}	3.9×10^{-2}	-	
	0.050	1.91×10^{-3}	3.8×10^{-2}		
	0.075	2.91×10^{-3}	3.8×10^{-2}		

Both rate and recovery were enhanced with the increase of Fe^{3+}. A significant rate increase was observed after increasing the Fe^{3+} solution content. At 25 °C, 8% Cu was obtained after 540 min (Figure 4), at a Fe^{3+} content of 0.025 M. The dissolution increased to 12% after 420 min with a Fe^{3+} concentration of 0.05 M. It increased further to 22% after 320 min at a Fe^{3+} concentration of 0.075 M. At 50 °C, Cu dissolution rate appeared to have doubled for each Fe^{3+} concentration increase (0.025, 0.050 and 0.075 M). This result suggests that the dissolution of Cu is related to both the Fe^{3+} concentration and temperature.

3.4. Residues Characterisation

Figure 5 shows the mineral content of the leached residues at 50 °C for the various pH conditions (1.0, 1.5 and 1.8) and compares their evolution to the feed sample. It was observed that the $CuFeS_2$ leached residue main peaks (2θ: 29.46, 48.93 and 57.95) appeared to have decreased in their intensity compared to the feed sample. In addition, the XRD analysis revealed that the other copper phases different from $CuFeS_2$ also dissolved and contributed to the overall Cu recovery. It was observed that anilite (Cu_7S_4) and digenite (Cu_9S_5) disappeared during the dissolution (Figure 5a–c), their contribution to the overall Cu dissolution if completely dissolved is 5% Cu. At pH 1.8, the total Cu was 24.7%, suggesting that Cu from $CuFeS_2$ also dissolved. Further, new copper sulphide phases were observed in the leached residues. These phases were low and inexistent in the feed sample and included chalcocite (Cu_2S) and covellite (CuS). These new phases could be attributed to the dissolution of $CuFeS_2$ by forming intermediate phases. The presence of these Cu-rich intermediates appeared to support an earlier investigation by Acero et al. [30] which underlined the preferential dissolution of Fe over Cu, leading to the formation of a Fe deficient chalcopyrite mineral (defect chalcopyrite structure $Cu_{1-x}Fe_{1-y}S_{2-z}$) to which our identified species could be part.

The covellite (CuS, 2θ: 28.75, 34.36 38.84 and 48.36) phase appeared to cumulate through the dissolution, suggesting its refractoriness as it has encapsulated the unreacted $CuFeS_2$ mineral, causing the dissolution to cease. The phases of the gypsum (Gy, 2θ: 11.69 & 20.81) and sulphur (So 2θ: 23.47, 40.71 and 50.19) were identified in all solid residues. The former (Gy) could be related to the carbonatite host rock. Its content appeared to increase with increasing media pH. The obtained results contradict those obtained by Tshilombo and Ojumu [28], who highlighted gypsum's presence, preventing further oxidation and mineral surface availability to the leach solution. Our results have shown that despite the presence of $CaSO_4$-H_2O, its effect on the dissolution was minimal since its content increases with increased pH value, at which better Cu dissolution was observed. S^0 is attributed to the dissolution reaction product (Equation (3)), as also reported in the studies conducted by Hammer et al. [31] and Sokic et al. [32]. Goethite and jarosite would be formed through the hydrolysis of Fe during leaching. Again, these two phases increased with increasing media pH value at which high Cu recoveries were obtained and could suggest that their effect on hindering Cu dissolution was negligible.

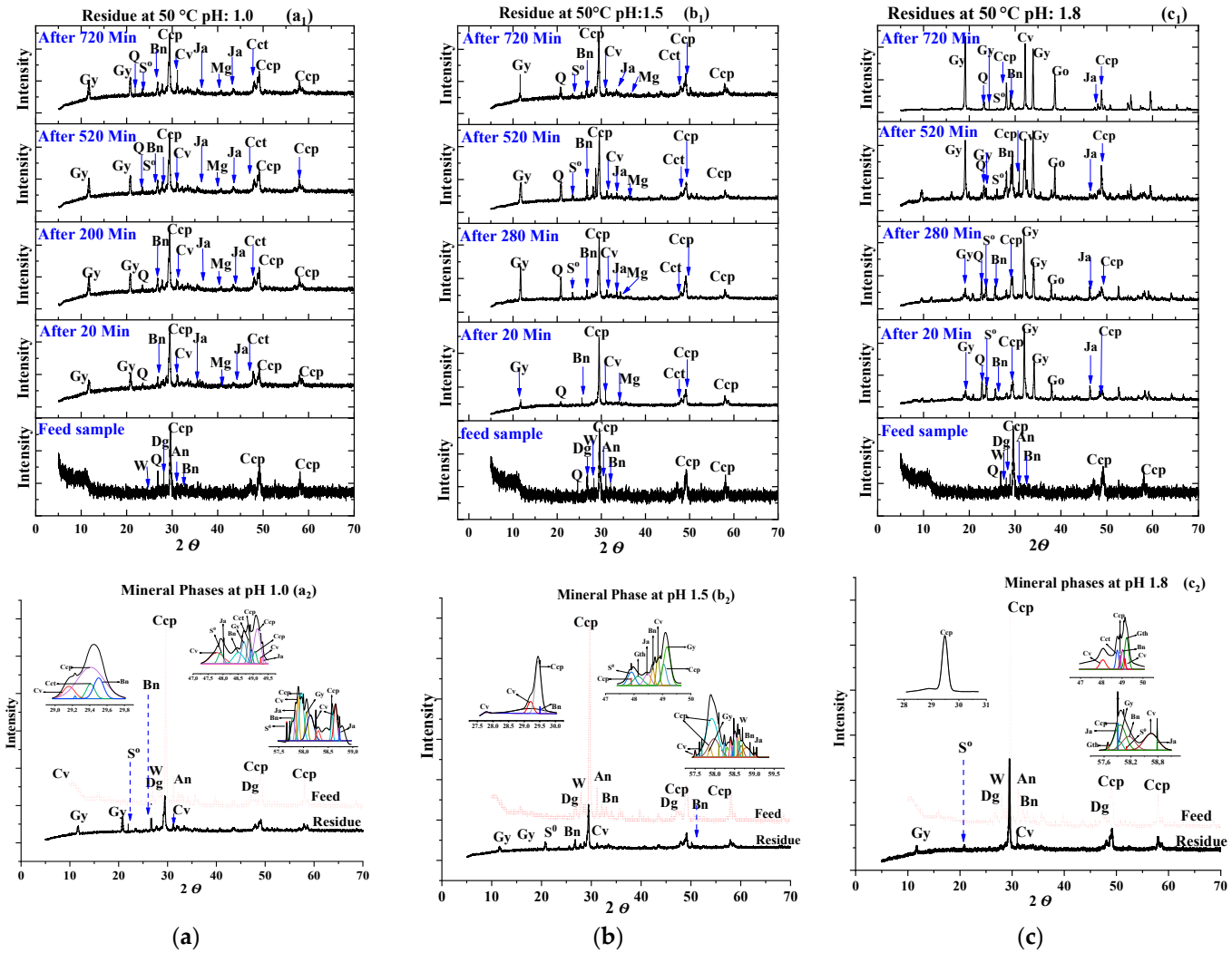

Figure 5. Diffraction patterns at the various pH condition at 50 °C, mineral phases evolution and interactions. Peak decomposition of main $CuFeS_2$ supporting the presence of intermediates phases. (**a**) summarises the solid residue's mineral phases at pH 1.0 while (**b**,**c**) displays the mineral phases at pH 1.5 and 1.8, respectively. Gy: gypsum, So: sulphur, Cv: covellite, Cct: chalcocite, Ccp: chalcopyrite, Bn: bornite, Mg: magnetite, Gth: goethite and Ja: jarosite.

Thermodynamics could assist by predicting the formation of the various observed phases and supporting their existence. In addition, it could assist with the determination of the dissolution pathway model based on the solid phase changes. Bornite appears to be the most favourable phase formed (Equation (4)), followed by chalcocite (Equation (3)) and, lastly, covellite (Equation (2)). The equations for the formation of copper intermediate phases and the energies involved (i.e., ΔG in kcal) are as follows:

$$CuFeS_2 + Fe_2(SO_4)_3 \rightleftharpoons CuS + 3FeSO_4 + S \quad \Delta G = -18.6 \tag{2}$$

$$2CuFeS_2 + 2Fe_2(SO_4)_3 \rightleftharpoons Cu_2S + 6FeSO_4 + 3S \quad \Delta G = -30.8 \tag{3}$$

$$5CuFeS_2 + 4Fe_2(SO_4)_3 \rightleftharpoons Cu_5FeS_4 + 12FeSO_4 + 6S \quad \Delta G = -68.7 \tag{4}$$

These Cu-S phases could react further into new Cu-S richer (Equations (5)–(8)) or leach to promote Cu recovery (Equations (8)–(10)). CuS is likely to form from Cu_5FeS_4 than Cu_2S. Similarly, Dutrizac et al. [33] and Zhao et al. [28] also reported the presence of CuS due to a transient species during the ferric leaching of Cu_5FeS_4. Cu_2S could also evolve and produce CuS (Equation (7)). Cu_5FeS_4 preferably dissolves before Cu_2S, which also

dissolves before CuS (Equation (10)). In addition to that, the covellite phase appeared as phase mutation of bornite during the withdrawal of Cu.

The reaction involved of intermediate phase mutation/alterations and the change in energy (i.e., ΔG in kcal) are as follows:

$$Cu_5FeS_4 + Fe_2(SO_4)_3 \rightleftharpoons 2.5Cu_2S + 3FeSO_4 + 1.5S \quad \Delta G = -8.00 \tag{5}$$

$$Cu_5FeS_4 + 2Fe_2(SO_4)_3 \rightleftharpoons 4CuS + 5FeSO_4 + CuSO_4 \quad \Delta G = -22.14 \tag{6}$$

$$2Cu_2S + Fe_2(SO_4)_3 \rightleftharpoons 2CuS + 2FeSO_4 + Cu_2SO_4 \quad \Delta G = +4.42 \tag{7}$$

Then, the dissolution of intermediate phases for complete copper dissolution process and energy changes (i.e., ΔG in kcal) follows:

$$CuS + Fe_2(SO_4)_3 \rightleftharpoons 2FeSO_4 + S + CuSO_4 \quad \Delta G = +2.12 \tag{8}$$

$$Cu_2S + 2Fe_2(SO_4)_3 \rightleftharpoons 4FeSO_4 + S + 2CuSO_4 \; \Delta G = -2.25 \tag{9}$$

$$2Cu_2S + Fe_2(SO_4)_3 \rightleftharpoons 2CuS + 2FeSO_4 + Cu_2SO_4 \quad \Delta G = +4.42 \tag{10}$$

Finally, the steps and energy change in phase formation related to gangue mineral (ΔG in kcal) is represented with the equation:

$$CaCO_3 + H_2SO_4 \rightleftharpoons CaSO_4 + H_2O + CO_2 \quad \Delta G = -32.1 \tag{11}$$

Figure 6 summarizes the solid-state dissolution process, based on the thermodynamics dissolution reactions, the evolution and interactions of the various copper phases observed during Cu leaching from the sulphide concentrate sample (XRD-RIR phase quantification) at pH 1.8 and a temperature of 50 °C. It was found that the rich traces of copper sulphide, including Cu_7S_4 and Cu_9S_5, were completely dissolved. The results suggest that most of the existing $CuFeS_2$ have been converted to its intermediate phases: Cu_5FeS_4, Cu_2S and CuS (Equations (2)–(4)).

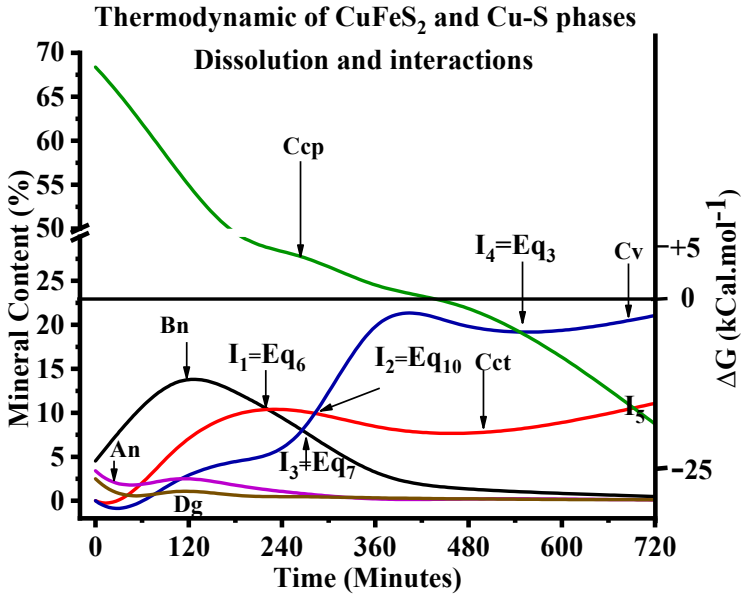

Figure 6. Solid-state dissolution process at 50 °C and pH of 1.8. Bo: bornite, An: anilite, Dg: digenite, Cct: chalcocite, Ccp: chalcopyrite and Cv: covellite.

The points of intersection in between the different transient phases could suggest, on the one hand, the competition of dissolution between the phases. Alternatively, it could also be attributed to the transformation from one phase to another. In this sense, I1 observed between Cu_5FeS_4 and Cu_2S could suggest that Cu_5FeS_4 was converted into

the Cu_2S phase (Equation (6)). While I2 for CuS and Cu_2S could be attributed to the competition of dissolving Cu among both phases, eventually, Cu_2S would dissolve since it is much soluble than CuS (Equations (9) and (10)). I3 observed for Cu_5FeS_4/CuS and Cu_2S/CuS could suggest that Cu dissolves from the Cu_5FeS_4 phase through the formation of CuS (Equation (7)). Finally, I4 is attributed to the strict conversion of $CuFeS_2$ into CuS without dissolving Cu (Equation (3)). The CuS phase appears to be more refractory than the other intermediates. Figure 7 presents and supports its cumulative behaviour throughout the dissolution.

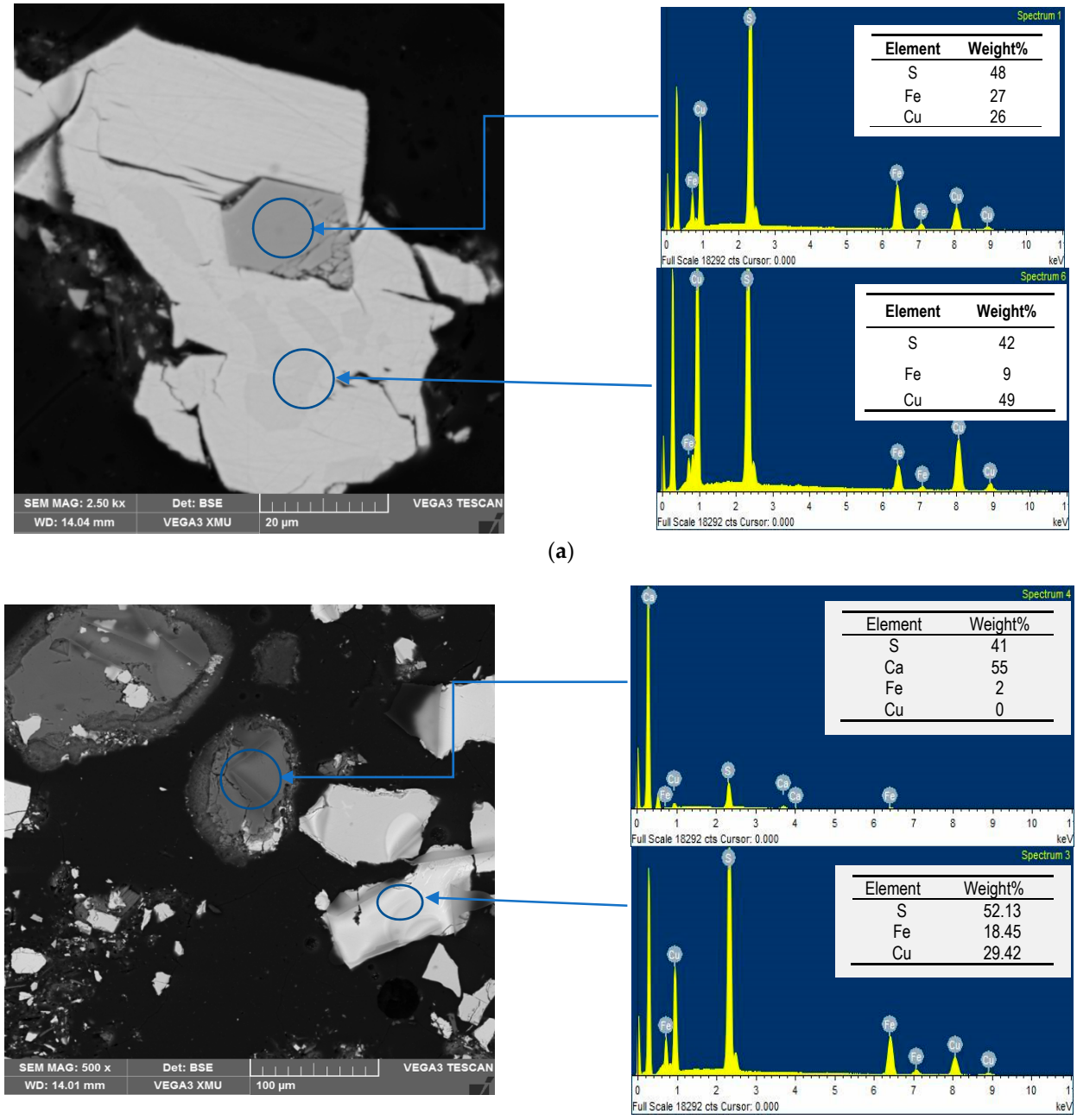

Figure 7. Leached residues morphology and chemistry (SEM-EDS): (**a**) displaying the mounted sample where the $CuFeS_2$ is locked or enveloped by Cu rich intermediate phases (Cu-S); (**b**) showing the unmounted sample where the Ca phase (Gypsum) represents the dissolution barrier.

Figure 7 summarizes the morphology and the relative weight fraction of Cu, Fe and S of 12 H solid residue. In all cases, both S and Cu have increased relative to Fe. This confirms the preferential dissolution of Fe over Cu and supports the presence of the Cu-S intermediate phase. S^0 was not identified under SEM-EDS as earlier reported by previous authors [29]. This could be because the residual solids were mounted, and the S^0 could have been removed through polishing. However, the SEM-EDS results showed that the dissolution could have been hindered by intermediates species, reaction products and gangue minerals. Figure 7 displays an intermediate species enveloping the chalcopyrite mineral, due to the low content of Fe (Figure 4a EDS results), this phase could be covellite mineral (CuS). Our results support those obtained earlier by Nyembwe and co-workers [34], who identified CuS as the refractory Cu-rich phase. In addition to that, micrograph C showed gypsum coating the surface of Cu sulphide and could also act as a dissolution barrier.

4. Conclusions

This work investigated the dissolution of a copper sulphide concentrate in acidic $Fe_2(SO_4)_3$. The dissolution reaction displayed is first order with respect to the $Fe_2(SO_4)_3$ within the investigated range (0.025–0.075 M). The solution speciation showed that Fe^{3+} and its complexes ($Fe(HSO_4)^{2+}$, $Fe(SO_4)^{2-}$ and $FeSO_4^{+}$) are responsible for Cu dissolution from $CuFeS_2$, leaching in H_2SO_4-$Fe_2(SO_4)_3$-$FeSO_4$-H_2O. The fast and linear first dissolution stage was attributed to the combined effect of Fe^{3+} and its complexes ($Fe(HSO_4)^{2+}$, while $Fe(SO_4)^{2-}$ was the main species for the second Cu dissolution stage characterised by a slow rate. The dissolution of $CuFeS_2$ is accompanied by intermediate phases which could either dissolve or evolve into bornite, chalcocite and covellite, in which covellite was identified as refractory and was also found to envelop the unreacted $CuFeS_2$ phase. Fe precipitates (goethite and jarosite) with gypsum appeared to have little effect on Cu dissolution hindrance.

Supplementary Materials: The following are available online at https://www.mdpi.com/article/10.3390/min11090963/s1, Figure S1: Potential-pH diagram of the Cu-Fe-S-H_2O system, Figure S2: Chalcopyrite bulk chemistry, mineral content grain morphology and particle size distribution, Figure S3: Set up of the leaching experiment showing picture of the actual overhead stirrer used in the experiments and the illustration of the apparatus set up, Table S1: The thermodynamic functions (ΔG^0 and S^0) and the equilibrium constants for the various iron species at 25, 35, 50 and 70 °C. Source references., Table S2: The conditions for kinetics investigation and the rates obtained at pH 1.8 media.

Author Contributions: Conceptualization, E.F.-K. and K.J.N.; methodology, E.F.-K., M.M. and K.J.N.; software, E.F.-K., M.M. and K.J.N.; validation, M.M., F.W. and E.F.-K.; formal analysis, K.J.N.; investigation, K.J.N., E.F.-K. and M.M.; resources, E.F.-K., F.W. and M.M.; data curation, K.J.N.; writing—original draft preparation, K.J.N.; writing—review and editing, M.M.; visualization, K.J.N.; supervision, E.F.-K. and M.M.; project administration, E.F.-K. and F.W.; funding acquisition, E.F.-K. and M.M. All authors have read and agreed to the published version of the manuscript.

Funding: This research was funded by National Research Foundation (NRF) in South Africa, grant number 120323.

Institutional Review Board Statement: Not applicable.

Informed Consent Statement: Not applicable.

Data Availability Statement: The data presented in this study are available on request from the corresponding author. The data are not publicly available due to intellectual property issues, including patent related and continuation of the research work.

Acknowledgments: We thank the support from the NSERC-DG, Research Nova Scotia, CFI, NSRIT, ACOA and NRC-IRAP in Canada.

Conflicts of Interest: The authors declare no conflict of interest.

References

1. Li, Y.; NKawashima, N.; Li, J.; Chandra, A.P.; Gerson, A.R. A review of the structure, and fundamental mechanisms and kinetics of the leaching of chalcopyrite. *Adv. Colloid Interface Sci.* **2013**, *197*, 1–32. [CrossRef] [PubMed]
2. Rodriguez, F.; Moraga, C.; Castillo, J.; Edelmira, G.; Robles, P.; Toro, N. Submarine Tailings in Chile—A Review. *Meatls* **2008**, *11*, 780.
3. Lundström, M.; Aromaa, J.; Forsén, O.; Barker, M.H. Reaction product layer on chalcopyrite in cupric chloride leaching. *Can. Metall. Q* **2008**, *47*, 245–252. [CrossRef]
4. Olvera, O.G.; Rebolledo, M.; Asselin, E. Atmospheric ferric sulfate leaching of chalcopyrite: Thermodynamics, kinetics and electrochemistry. *Hydrometallurgy* **2016**, *165*, 148–158. [CrossRef]
5. Dutrizac, J.E. Elemental sulphur formation during the ferric chloride leaching of chalcopyrite. *Hydrometallurgy* **1990**, *23*, 153–176. [CrossRef]
6. Veloso, T.C.; Peixoto, J.J.M.; Pereira, M.S.; Leao, V.A. Kinetics of chalcopyrite leaching in either ferric sulphate or cupric sulphate media in the presence of NaCl. *Int. J. Miner. Process.* **2016**, *148*, 147–154. [CrossRef]
7. Nikkhou, F.; Xia, F.; Deditius, A.P. Variable surface passivation during direct leaching of sphalerite by ferric sulfate, ferric chloride, and ferric nitrate in a citrate medium. *Hydrometallurgy* **2019**, *188*, 201–215. [CrossRef]
8. Tshilombo, A.F. *Mechanism and Kinetics of Chalcopyrite Passivation and Depassivation during Ferric and Microbial Leaching*; The University of British Columbia: Vancouver, BC, Canada, 2004. [CrossRef]
9. Naderi, H.; Abdollahy, M.; Mostoufi, N.; Koleini, M.; Shojaosadati, S.A.; Manafi, Z. Kinetics of chemical leaching of chalcopyrite from low grade copper ore: Behavior of different size fractions. *Int. J. Miner. Met. Mater.* **2011**, *18*, 638–645. [CrossRef]
10. Klauber, C.; Parker, A.; Van Bronswijk, W.; Watling, H. Sulphur speciation of leached chalcopyrite surfaces as determined by X-ray photoelectron spectroscopy. *Int. J. Miner. Process.* **2001**, *62*, 65–94. [CrossRef]
11. Salehi, S.; Noaparast, M.; Ziaeddin, S. The role of catalyst in chalcopyrite passivation during leaching. *Int. J. Min. Geo-Eng.* **2017**, *1*, 91–96.
12. Debernardi, G.; Carlesi, C. Chemical-electrochemical approaches to the study passivation of chalcopyrite. *Miner. Process. Extr. Met. Rev.* **2013**, *34*, 10–41. [CrossRef]
13. Ghahremaninezhad, A. The Surface Chemistry of Chalcopyrite during Electrochemical Dissolution. Ph.D. Thesis, The University of British Columbia, Vancouver, BC, Canada, 2012.
14. Zhao, H.; Zhang, Y.; Zhang, X.; Qian, L.; Sun, M.; Yang, Y.; Zhang, Y.; Wang, J.; Kim, H.; Qiu, G. The dissolution and passivation mechanism of chalcopyrite in bioleaching: An overview. *Miner. Eng.* **2019**, *136*, 140–154. [CrossRef]
15. Ruiz-sánchez, A.; Lapidus, G.T. Hydrometallurgy Study of chalcopyrite leaching from a copper concentrate with hydrogen peroxide in aqueous ethylene glycol media. *Hydrometallurgy* **2017**, *169*, 192–200. [CrossRef]
16. Casas, J.M.; Crisóstomo, G.; Cifuentes, L. Speciation of the Fe(II)-Fe(III)-H_2SO_4-H_2O system at 25 and 50 °C. *Hydrometallurgy* **2005**, *80*, 254–264. [CrossRef]
17. Yue, G.; Asselin, E. Kinetics of Ferric Ion Reduction on Chalcopyrite and Its Influence on Leaching up to 150 °C. *Electrochim. Acta* **2014**, *146*, 307–321. [CrossRef]
18. Hirato, T.; Majima, H.; Awakura, Y. The leaching of chalcopyrite with ferric sulfate. *Met. Mater. Trans. A* **1987**, *18*, 489–496. [CrossRef]
19. Sapieszko, R.S.; Patel, R.C.; Matijevic, E. Ferric hydrous oxide sols. 2. Thermodynamics of aqueous hydroxo and sulfato ferric complexes. *J. Phys. Chem.* **1977**, *81*, 1061–1068. [CrossRef]
20. Simons, K. *Soil Sampling*; Gilson, Inc.: Geogia, GA, USA, 2014.
21. Nyembwe, K.J.; Fosso-Kankeu, E.; Waanders, F.; Nyembwe, K.D. Structural, compositional and mineralogical characterization of carbonatitic copper sulfide: Run of mine, concentrate and tailings. *Int. J. Miner. Metall. Mater.* **2019**, *26*, 143–151. [CrossRef]
22. Antonijevic, G.D.; Bogdanovic, M.M. Investigation of the leaching of chalcopyritic ore in acidic solutions. *Hydrometallurgy* **2004**, *73*, 245–256. [CrossRef]
23. Córdoba, E.M.; Muñoz, J.A.; Blázquez, M.L.; González, F.; Ballester, A. Leaching of chalcopyrite with ferric ion. Part I: General aspects. *Hydrometallurgy* **2008**, *93*, 81–87. [CrossRef]
24. Salinas, K.E.; Herreros, O.; Torres, C.M. Leaching of Primary Copper Sulfide Ore. *Mineral* **2018**, *8*, 312. [CrossRef]
25. Jones, D.L.; Peters, E. *Extractive Metallurgy of Copper*; AIME: New York, NY, USA, 1976.
26. Hirato, T.; Majima, H.; Awakura, Y. The leaching of chalcopyrite with cupric chloride. *Met. Mater. Trans. A* **1987**, *18*, 31–39. [CrossRef]
27. Striggow, B. *Field Measurement of Oxidation-Reduction Potential (ORP)*; United States Environmental Protection Agency: Georgia, GA, USA, 2013.
28. Zhao, H.; JWang, J.; Qin, W.; Hu, M.; Qiu, G. Electrochemical dissolution of chalcopyrite concentrates in stirred reactor in the presence of Acidithiobacillus ferrooxidans. *Int. J. Electrochem. Sci.* **2015**, *10*, 848–858.
29. Sokić, M.D.; Marković, B.; Živković, D. Kinetics of chalcopyrite leaching by sodium nitrate in sulphuric acid. *Hydrometallurgy* **2009**, *95*, 273–279. [CrossRef]
30. Acero, P.; Cama, P.; Ayora, J.; Asta, C.M. Chalcopyrite dissolution rate law from pH 1 to 3. *Geol. Acta* **2009**, *7*, 389–397.
31. Harmer-bassell, S.L.; Thomas, J.E.; Harmer, S.L.; Thomas, J.E. The evolution of surface layers formed during chalcopyrite leaching The evolution of surface layers formed during chalcopyrite leaching. *Geochim. Cosmochim. Acta* **2006**, *70*, 4392–4402. [CrossRef]

32. Sokic, M.D.; Markovic, B.R.; Matkovic, V.L.; Strbac, N.D.; Zivkovic, D.T. Mechanism of Chalcopyrite Leaching in Oxidative Sulphuric Acid Solution. *J. Chem. Chem. Eng.* **2011**, *5*, 37–41.
33. Dutrizac, J.E.; Chen, T.T.; Jambor, J.L. Mineralogical changes occurring during the ferric lon leaching of bornite. *Met. Mater. Trans. A* **1985**, *16*, 679–693. [CrossRef]
34. Nyembwe, K.J.; EFosso-kankeu, E.; Waanders, F.; Mkandawire, M. pH-dependent leaching mechanism of carbonatitic chalcopyrite in ferric sulfate solution. *Trans. Nonferrous Met. Soc. China* **2021**, *31*, 2139–2152. [CrossRef]